Published in final edited form as:
Biomaterials. 2012 April ; 33(10): 2952–2960. doi:10.1016/j.biomaterials.2011.12.043.

Internalization of C60 fullerenes into cancer cells with accumulation in the nucleus via the nuclear pore complex

Mustafa Raoof[1], **Yuri Mackeyev**[2], **Matthew A. Cheney**[2], **Lon J. Wilson**[2], and **Steven A. Curley**[*,1,3]

[1]Department of Surgical Oncology, The University of Texas M. D. Anderson Cancer Center, Houston, TX, USA

[2]Department of Chemistry and Richard E. Smalley Institute for Nanoscale Science & Technology, Rice University, Houston, TX, USA

[3]Department of Mechanical Engineering and Materials Science Rice University, Houston, TX, USA

Abstract

A highly water-soluble, non-ionic, and non-cytotoxic fullerene malonodiserinolamide-derivatized fullerene C_{60} (C_{60}-ser) is under investigation as a potential nanovector to deliver biologic and cancer drugs across biological barriers. Using laser-scanning confocal microscopy and flow cytometry, we find that PF-633 fluorophore conjugated C_{60}-ser nanoparticles (C_{60}-serPF) are internalized within living cancer cells in association with serum proteins through multiple energy-dependent pathways, and escape endocytotic vesicles to eventually localize and accumulate in the nucleus of the cells through the nuclear pore complex. Furthermore, in a mouse model of liver cancer, the C_{60}-serPF conjugate is detected in most tissues, permeating through the altered vasculature of the tumor and the tightly-regulated blood brain barrier while evading the reticulo-endothelial system.

Keywords

fullerenes; nucleus; cancer; liver; nuclear pore complex; subcellular localization; biodistribution

INTRODUCTION

Fullerenes are carbon cages with nanosized dimensions and an aesthetic symmetry that has fascinated scientists since their discovery in 1985(1). Biological use of pristine C_{60} is limited by its insolubility in aqueous environments. The motivation to exploit size, geometry and molecular topology for therapeutic applications has resulted in the synthesis and

[*]Corresponding author: Steven A. Curley, M.D, UT M. D. Anderson Cancer Center, Department of Surgical Oncology, Unit 1484, P.O. Box 301402, Houston, TX 77230-1402, Phone: 713-794-4957, Fax: 713-745-5235 .
Mustafa Raoof: mraoof@mdanderson.org
Yuri Mackeyev: mackeyev@rice.edu
Matthew A. Cheney: mac5@rice.edu
Lon J. Wilson: durango@rice.edu
Steven A. Curley: scurley@mdanderson.org

characterization of a number of water-soluble fullerene derivatives. It is not surprising to note that amidst concerns of toxicity, the list of potential biological application of these derivatized carbon-structures continues to grow to include drug delivery agents(2, 3), gene therapy agents (4, 5), photodynamic(6-9) and photoacoustic(10) cancer therapy agents, as antioxidants(11), radioprotection agents (12, 13) and diagnostic contrast agents(14, 15).

The use of derivatized, water-soluble, non-toxic fullerenes is of particular interest to us in designing nanovectors for cancer therapeutics. The fullerene cage offers a unique three-dimensional scaffold for covalent attachment of multiple drugs for single-dose combination therapy and thus, has a clear advantage over many other nanovectors that utilize non-covalent loading, embedding, or encapsulation strategies. For instance, in separate studies, C_{60}-paclitaxel and C_{60}-doxorubicin conjugates were designed as a slow-release formulation that significantly enhanced the bioavailability and therapeutic efficacy of paclitaxel and doxorubicin against lung cancer cells and melanoma tumors, respectively(2, 3). Despite their immense potential as nanovectors, studies on transport of derivatized fullerenes in cancer cells and in relevant pre-clinical tumor models are limited. One of the main challenges to the study of biodistribution and subcellular localization is the difficulty in detecting individual fullerene-derivatized nanoparticles (NPs). Using metal, fluorophore, or radioisotope-tagged fullerene derivatives, several reports have documented cellular uptake and subcellular localization via endocytotic processes. For instance, separate studies have demonstrated that malonic acid derivatized $C_{60}C(COOH)_2$ and $C_{63}(COOH)_6$ localize predominantly to the mitochondria(16, 17) and the bis-adduct, $C_{60}(C(COOH)_2)_2$ localized to lysosomes(18). In another report, an amine-functionalized C_{70}-Texas Red conjugate was found to co-localize mostly with the endoplasmic reticulum and to a lesser extent with the lysosomes and mitochondria of mast cells(19). A cumulative assessment of these reports suggests that subcellular localization of derivatized-fullerenes is dependent on the nature of functionalization and possibly the type of cells investigated. Both observations are attractive avenues for further study, as there is the potential to target cancer cells and specific subcellular locations of interest by fullerene cage modification.

The synthesis and characterization of highly water-soluble, non-ionic and functionalized derivatives of C_{60} have been previously reported(20). Our current investigation pertains to the cellular transport of a malonodiserinolamide-derivatized fullerene C_{60} (C_{60}-ser) in liver cancer cells. In order to study the processing of C_{60}-ser by liver cancer cells, C_{60}-ser has been covalently attached to the fluorophore, promofluor 633 (to produce C_{60}ser-PF) with an emission spectrum at >600 nm to produce minimal interference with cell auto-fluorescence and absorption by the C_{60} core. The conjugate was synthesized using an amide-linkage to protect against hydrolases within the cell (Figure 1, S1 and S2). Using laser-scanning confocal microscopy and flow cytometry, we investigate the cellular localization and mechanism of uptake of C_{60}-serPF in liver cancer cells. Furthermore, we evaluate the biodistribution of these nanoparticles in a mouse model of liver cancer.

MATERIALS & METHODS

Synthesis and characterization of C_{60}-serPF conjugate

C_{60}-ser has been prepared as described previously(15). C_{60}-serPF has been synthesized and purified according to the procedure described in the Supporting Information. A scheme is represented in Figure 1.

Materials, cell culture and cell lines

We obtained the Hep3B cell line from American type culture collection (ATCC) and the Huh-7 cell line was a kind gift from Dr. Felipe Samaniego (M.D. Anderson Cancer Center).

Cells were maintained in MEM cell culture media and 10% fetal bovine serum, supplemented with sodium pyruvate, non-essential amino acids and penicillin G / streptomycin (GIBCO). The cells were grown in 150cm^2 flasks placed in a humidified incubator at 37°C with 5% CO_2 before experimental use. The following inhibitors were used (all from Sigma-Aldrich, Milwaukee, WI); Chlorpromazine (50μM), di-methyl amiloride (DMA, 100μM), Methyl β-cyclodextrin (MBCD, 10mM), Nystatin (50μM), Dynasore (80μM), Thapsigargin (0.5μM).

Cytotoxicity studies

Cytotoxicity was assessed using propidium iodide staining. Promidium iodide is extruded from viable cells. After varying duration and concentrations of exposure to C_{60}-ser, C_{60}-serPF, or PF633, cells were trypsinized and washed with PBS. Approximately 0.3ml of PI/RNase solution was added to cells (BD Pharmingen, San Diego, CA). Cells were incubated on ice for 15 minutes and analyzed using Flow cytometry (BD LSR II, BD Biosciences, San Jose, CA).

Laser-scanning confocal microscopy analysis

For confocal microscopy experiments, cells were grown on #1.5 round cover slips in 12-well plates at approximately 50,000 cells per well. After 24 hours sub-confluent monolayers were observed. Cells were washed with phosphate-buffered saline (PBS) once and then incubated at the desired concentration of C_{60}-serPF for varying duration. At the end of incubation period, cells were washed with PBS and fixed in 1% Paraformaldehyde for 30 minutes, then washed again and stained with 4′, 6-diamidino-2-phenylindole (DAPI, Invitrogen, Carlsbad, CA). The cover slips were placed on microscopy slides with a drop of Gold anti-fade reagent (Invitrogen) and sealed. Imaging was performed with Olympus Laser-scanning FV500 microscope using a 60x oil objective and a Z-stack resolution set at 100nm. Fixed cells were excited with a 405nm laser and a red 633nm HeNe laser and emission recorded at 470nm and 660nm respectively in sequential steps to prevent bleed-through and photo-bleaching. Images were analyzed in Slidebook (v5.0)

Nuclear extraction and flow cytometry analysis

After incubation with C_{60}-serPF for varying duration cells were washed with PBS and re-suspended in ice-cold nuclei extraction buffer (sucrose (320mM), MgCl2 (5mM), Hepes (10mM), Triton (1% v: v) was mixed and pH adjusted to 7.4), vortexed for 10 seconds, and incubated on ice for 10 minutes. Nuclei were then pelleted at 2000g for 5min and re-suspended in wash buffer (same as nuclei extraction buffer but without triton). This was repeated twice and nuclear extraction was confirmed by bright-field microscopy and trypan blue staining. The extracted nuclei were then stained with propidium iodide for 15 minutes before flow cytometry analysis. Single-parameter (nuclear localization studies) and multi-parameter (cell cycle studies) flow cytometry analysis was performed using a BD LSR II FACS (Beckton Dickinson, Franklin Lakes, NJ). For C_{60}-serPF detection, nuclei or cells were excited with 640nm SORP Red Laser and emission was recorded at 635-684nm. For DNA content measurements, propidium iodide fluorescence was recorded at 570-597nm after excitation with a 561nm laser. To measure internalization of C_{60}-serPF, approximately 1 million cells were incubated with or without pharmacological inhibitors for 45 minutes on ice in cell culture media as described above. C_{60}-serPF was then added and cells were restored to 37°C. Aliquots (50μL) were removed at various time points and fluorescence was measured as described above. At t = 0 min, cells exposed to the conjugate were immediately assessed to calculate the background signal due to passive adsorption of C_{60}-serPF.

Animal experiments

A mouse model of liver cancer was generated using 4 wk old CB17 SCID mice. Animals were anesthetized using isoflurane and a transverse incision was made in the upper abdomen under sterile conditions. Approximately 1.5 million Hep3B cells were injected in the liver in a 10μL volume (Hamilton Syringes). Hemostasis was restored using gentle pressure and silver nitrate cautery. Biodistribution experiments were conducted 4 weeks after injection. C_{60}-serPF was injected in the dorsal tail vein. Animals were sacrificed at various time points starting at 16 hours and tissues were harvested for fluorescence imaging and histology. Fluorescence imaging was performed on harvested tissues immediately, with Xenogen optical in vivo imaging system (IVIS 200, Caliper Life Sciences, Hopkinton, MA) and using Cy5.5 excitation (615-665nm) and emission (695-770nm) filter set.

RESULTS

C_{60}-serPF localization in liver cancer cells

Laser-scanning confocal microscopy was used to study fluorescently labeled C_{60}-serPF uptake in human liver cancer cells. We exposed Hep3B and Huh7 cells to varying concentrations of C_{60}-serPF for 2 hours and the cells were fixed for imaging. As shown in figure 2 and S3, a dose-dependent uptake was observed in a linear fashion. We observed that at lower concentrations, 78±8 % of the total fluorescence intensity from each cell localized to the cytosol. However, at higher concentrations this proportion decreased to approximately 50%. Conversely, nuclear uptake increased from 22± 8% at 1 μg/ml to 47± 5% at 100 μg/ml. Similar observations were obtained with Huh-7 cells. Since the relative physical dimensions of the nucleus and cytoplasm vary in each cell, we calculated the sum fluorescence intensity per μm^3 from the nucleus and the cytoplasm of each cell. As shown in figure 2A (bottom, left), C_{60}-serPF preferentially accumulated in the nucleus, reaching concentrations up to three times that in the cytoplasm at higher incubation concentrations. In order to evaluate the integrity of the conjugate within the nucleus, we measured fluorescence-decay of free PromoFluor-633 dye and C_{60}-serPF conjugate in separate experiments. The half-life of the free PromoFluor was 54 seconds and that of C_{60}-serPF was 146 seconds in the nucleus. The fluorescence decay observed is comparable to the decay observed when the compounds are loaded in Sephadex microbeads and subjected to photo-bleaching (Figure S4). These findings imply that the C_{60}-serPF conjugate remains intact in the cellular environment.

In order to quantify the proportion of cells with uptake in the nucleus, nuclei were extracted from unfixed cells after a two-hour exposure to C_{60}-serPF. The nuclear extraction procedure resulted in a yield of >97% as determined through microscopic analysis after trypan blue staining and a decrease in forward scatter on flow cytometry. As shown in figure 2B, 88% and 87% of the nuclei extracted from Hep3B and Huh7 cells were positive for C_{60}-serPF, respectively. This data is consistent with confocal microscopy observations that the majority of nuclei were observed to emit varying intensity of fluorescence signal above background.

We investigated whether nuclear localization could occur because of membrane permeabilization caused by cytotoxicity of the conjugate. Propidium iodide is a fluorescent cell impermeant dye that fluoresces after intercalating with nucleic acids in membrane-damaged cells. Our data demonstrated that C_{60}-ser, PF or C_{60}-serPF (each at 100μg/ml) did not cause cytotoxicity or permeabilization of membranes after 4 hours of exposure, while 0.3% (v:v) triton was sufficient to permeabilize the membranes after 15 minutes of exposure (Figure S5).

Dynamics of cellular uptake of C_{60}-serPF

The kinetics of cellular entry of C_{60}-serPF was studied using flow cytometry. Live Hep3B and Huh7 cells were exposed to C_{60}-serPF for varying durations under different conditions to elucidate the mechanism of uptake. As shown in figure 3, cellular uptake is a time-dependent process reaching a maximum at about 3 hours. The cellular uptake of C_{60}-serPF is also energy-dependent as incubation at 4°C significantly inhibited its entry into the cells. In order to investigate if conjugation of the promofluor to C_{60}-ser alters the cellular uptake mechanism, we pre-incubated the cells with C_{60}-ser at a 100-fold higher concentration for 1 hour. This process significantly inhibited the uptake of C_{60}-serPF in both liver cancer cell lines. These findings suggest a common pathway for cellular entry of C_{60}-ser and C_{60}-serPF.

Prior studies have reported association of C_{60}-derrivatives with several proteins by non-covalent interactions(21-23), so we determined if serum proteins aid in the cellular uptake of C_{60}-ser. The experiments were repeated with and without serum proteins and the rate of internalization was calculated over the first 2 hours of exposure to the C_{60}-serPF. As shown in figure 3B, the rate of C_{60}-serPF internalization reaches a plateau at a concentration of 10 μg/ml, suggesting a saturation of the cell's internalization mechanism. Cells suspended in serum-free media demonstrated delayed internalization kinetics, indicating that association of C_{60}-serPF with proteins facilitates cellular entry. Next, the subcellular localization of C_{60}-serPF after internalization was investigated. Time-lapse confocal microscopy images showed that upon entry C_{60}-serPF can be seen as punctate aggregates within the cytoplasm, resembling endocytotic vesicles, which progressively increase in intensity over the course of the first hour. Intense nuclear localization of C_{60}-serPF was observed later at 2-4 hours after treatment.

Pathway of cellular uptake

Several energy-dependent pathways have been characterized in living cells that are responsible for trans-membrane exchange of materials. We thus evaluated the major uptake mechanisms that are of known significance in non-immune eukaryotic cells namely, clathrin-mediated endocytosis, lipid raft/caveolae-mediated endocytosis, and macropinocytosis(24). These pathways have been characterized based on their differential sensitivity to pharmacological inhibitors. Concentrations of inhibitors that yield maximum inhibition without unwanted toxicity were utilized as published in prior reports and summarized in a recent review(25).

Internalization of C_{60}-serPF by liver cancer cells was found to be pan-sensitive to various inhibitors suggesting multiple pathways of uptake (Figure 4). First, the role of macropinocytosis in C_{60}-serPF internalization was investigated. Macropinocytosis involves formation of large F-actin coated vacuoles that require polymerization of the cell's actin machinery. The size of vacuoles, thus formed, is relatively large (>0.2 μm) and the vacuoles are inherently leaky allowing internalized cargo to escape into the cytosol(26). Dimethyl amiloride (DMA) has been shown to inhibit constitutive and stimulated macropinocytosis in a variety of eukaryotic cells(27, 28). We observed that C_{60}-serPF uptake was sensitive to inhibition by DMA in Hep3B and Huh7 cells, indicating that the internalization is partially dependent on macropinocytosis. Both clathrin and lipid-raft/caveolae-mediated uptake is dynamin-dependent while macropinocytosis is dynamin-independent(29, 30). Dynamin guanosine triphosphatase (GTPase) plays a critical role in pinching-off of the invaginations that form as a result of dynamin-dependent clathrin or caveolin-mediated processes(31). Dynasore is a small molecule GTPase inhibitor selective for dynamin(32). The data demonstrated significant, although incomplete, inhibition of C_{60}-serPF internalization by dynasore, implying that the uptake is also dependent on dynamin in part. In order to pinpoint the mechanism of dynamin-dependent uptake, cells were pre-incubated with a specific

inhibitor of clathrin-mediated uptake, chlorpromazine, or inhibitors of caveolin/lipid-raft-mediated uptake such as methyl-β-cyclodextrin (MBCD) or nystatin(33, 34). Chlorpromazine inhibition of clathrin-mediated endocytosis involves the loss of clathrin-adapter protein 2 complex, which is vital in invagination of clathrin-coated vesicle(35). Our results showed that while internalization of C_{60}-serPF was significantly inhibited in Hep3B cells by chlorpromazine, it was minimally inhibited in Huh7 cells. Conversely, inhibitors of lipid-raft/caveolin pathway were ineffective in inhibiting uptake of C_{60}-serPF in Hep3B cells while a significant inhibition was seen in Huh7 cells, suggesting a role for caveolin-mediated uptake. Irrespective of the internalization pathway, 2-4 hours after internalization the compartmentalized C_{60}-serPF conjugate escapes the endocytotic vesicles and 47± 5% of the total internalized conjugate localizes to the nucleus.

Mechanism of nuclear entry of C_{60}-serPF

During mitosis, the nuclear envelope is dissolved and reformed to allow division of nuclei. In an asynchronous sub-confluent culture of Hep3B and Huh7 cells, the proportion of cells undergoing mitosis at a given time is small (<30%) compared to those in G0/1 or S phase. Since a large majority of cells accumulate C_{60}-serPF in the nucleus within two hours of exposure, it is unlikely that the localization of C_{60}-serPF to the nucleus is highly dependent on the cell cycle phase. Nonetheless, we investigated this possibility. Hep3B or Huh-7 cells untreated or treated with C_{60}-serPF for two hours were evaluated based on their DNA content after extracting their nuclei. As shown in figure 5B, the relative distribution of nuclei in various phases of cell cycle is similar in treated and untreated cells. Relative change in the geometric mean fluorescence intensity after treatment with C_{60}-serPF in G0/1, S and G2/M phases was also similar (not shown) to suggest that nuclear localization is independent of the cell cycle phase.

The nuclear envelope is a complex double membrane structure that compartmentalizes the genetic material within the cell. Transport of water-soluble materials across this double layer is tightly regulated by the nuclear pore complex (NPC)(36). Molecules that are smaller than 25 kDa can pass through NPC by passive diffusion. Larger molecules however, require active transport(36). Both passive and active diffusion through NPC is calcium dependent(37). Calcium ions are actively pumped within the double layer through Ca^{2+}-ATPase located in the endoplasmic reticulum. The double layer of nuclear envelope is contiguous with the peri-nuclear endoplasmic reticulum. Inhibition of Ca^{2+}-ATPase by thapsigargin depletes calcium stores in the endoplasmic reticulum and within the nuclear envelope. Loss of calcium induces a steric block of the central and peripheral channels within the NPC(37). In our experiments, cells treated with thapsigargin showed complete inhibition of nuclear uptake of the C_{60}-serPF NPs. As shown in figure 5A, a signet ring-like appearance of fluorescence is seen around the nucleus representing internalized NPs in the cytosol with complete blockade of nuclear entry. It is not clear from this experiment if the transport of C_{60}-serPF is active or passive, since thapsigargin blocks both. However, while C_{60}-serPF is small enough (2.8 kDa) to navigate through the NPC by passive diffusion, active transport by association of C_{60}-serPF with cytosolic proteins that have nuclear localization signals cannot be excluded.

In order to test this hypothesis, we subjected the cells to hyperthermia at 42.5°C in the presence of C_{60}-serPF for 2 hours and nuclear uptake was assessed in isolated nuclei using flow cytometry (Figure 5C). This thermal dose has no effect on cell viability (data not shown). Nuclear protein content increased by 10-40% during hyperthermia as various adaptive processes are initiated and the cell prepares to respond to the heat shock(38). This increased protein content is secondary to re-localization of several cytosolic proteins, e.g. hsp70, to the nucleus through the nuclear pore complex(39). In the hyperthermia

experiment, nuclear uptake of C_{60}-serPF was enhanced from 80% to ~100% which supports the role of active transport through the NPC in association with cellular proteins.

Biodistribution of C_{60}-serPF *in vivo*

The data thus far suggest that C_{60}-serPF NPs by virtue of their high water solubility and association with proteins can cross multiple cellular barriers. An obvious and direct implication of these findings is in non-viral gene therapy, and the drug-delivery design of cancer therapeutics. We sought to investigate the biodistribution of C_{60}-serPF in a murine orthotopic Hep3B xenograft model of primary hepatocellular carcinoma. Fluorescence was measured from multiple organs at various time points after systemic administration of 5 mg/kg C_{60}-serPF.

The data shown in figure 6 demonstrates the relative biodistribution of C_{60}-serPF in various tissues. At 16 hours, the NPs primarily localized in the renal tissue, suggesting a predominant renal mechanism of clearance from the body. This was consistent with visual observations of change in color of the urine within 15 minutes of injection. The NPs also concentrated in the liver and the malignant liver tumor, which peaked at 48 hours and 16 hours after injection, respectively. A delayed uptake in the liver and a more delayed presence in pancreatico-biliary tree most likely represents delayed hepatic clearance of the redistributed NPs eliminated from the tissues. We also found significant uptake of C_{60}-serPF in the brain. This uptake of untargeted C_{60}-serPF is an exciting prospect for the use of fullerene agents as a drug delivery vector across the blood brain barrier, which will certainly require further study. Finally, these nanoparticles tend not to sequester in the spleen. One of the major challenges of nanovector-mediated drug delivery is evasion of the reticulo-endothelial system. It is likely that C_{60}-serPF NPs, by docking with serum proteins and by their small size (3-4 nm), are masked from immune detection. While C_{60}-serPF NPs are rapidly cleared after systemic administration because of their small size, a significant portion is retained and traverse most biological tissues including altered and tightly-regulated vascular beds of tumor and brain, respectively. Our efforts to study nuclear uptake *in vivo* in these tissues were met with challenges because of weak fluorescence and a poor signal to noise ratio on confocal microscopy.

DISCUSSION

Several aspects of this investigation merit further discussion. The key finding of this study is that C_{60}-serPF localizes to the nucleus of liver cancer cells. Although two reports have previously described nuclear localization of pristine fullerenes when administered in gallic acid (40, 41) or tetrahydrofuran-stabilized colloidal suspensions (41), their biological application as nanovectors is limited because of the inhomogeneity of the preparations and the toxic nature of these fullerene materials. The present work is the first report that describes the nuclear localization, with mechanistic details, of a non-cytotoxic, water-soluble derivative of C_{60}. Nuclear entry of nanovectors has far reaching potential since the nucleus is the intended target for most conventional cancer drugs and gene therapy. The findings of this study suggest that C_{60}-serPF exploits the cell's native mechanisms that transport proteins across various biological barriers. By docking with such proteins, fullerene-derivatized NPs such as C_{60}-serPF can persist in tissue for more than a week, evading immune recognition by the reticulo-endothelial system and entering the nucleus through the tightly-regulated nuclear pore complex.

Regarding cellular uptake, our findings are consistent with several prior studies that have implicated energy-dependent endocytotic pathways in the uptake of functionalized-fullerenes. Individual C_{60}-ser molecules are not sufficiently small to navigate across numerous ion-channels of the cell. Such an equilibration would be rapid, requiring only

minutes. The effective hydrodynamic diameter of individual C_{60}-serPF NPs (3-4 nm) precludes that possibility, since our study failed to show significant uptake in either cell line at 30 minutes after incubation with the NPs. Route of entry in the cell often correlates with the eventual subcellular location within the cell. For instance, Li et al. documented localization of functionalized-fullerenes to the lysosomes after well-characterized clathrin-mediated uptake and not through caveolin-mediated pathway(18). However, macropinocytosis was not assessed using pharmacological inhibitors in the Li study. Data for an amine-derivatized C_{70}-Texas Red conjugate demonstrated uptake in mast cells. However the results suggested that the process is susceptible to a variety of endocytosis inhibitors(19). In the present investigation we utilized the quantitative assessment of geometric mean fluorescence intensity to sample more than 5000 cells over the course of three hours in the presence or absence of various inhibitors. In our studies, it was noted that C_{60}-serPF uptake was also sensitive to a variety of inhibitors, demonstrating that the cellular uptake of C_{60}-serPF is dependent on multiple pathways that may vary in different cell lines and types. For instance, in Hep3B cells C_{60}-serPF internalization was predominantly through macropinocytosis and dynamin-dependent clathrin-mediated uptake and not through a lipid-raft or a caveolae-mediated pathway. Conversely, the uptake in Huh-7 cells was mediated through macropinocytosis and a dynamin-dependent, caveolin-mediated pathway but not through a clathrin-mediated pathway. These findings reflect biologically relevant underlying differences in the two cell lines. For instance, different cell lines vary in their membrane content of caveolin or clathrin(42, 43). Although we currently have no data on comparative analysis of membrane content of these structures, taken together, these findings suggest that cancer cell entry by C_{60}-serPF is non-specific and follows both dynamin-dependent and independent pathways. Since mammalian cells utilize multiple pathways to internalize different protein cargo, this could be explained on the basis of non-specific association of C_{60}-serPF with various proteins. Our data certainly suggests that the presence of proteins assists the entry of C_{60}-serPF into cells. Finally, it is important to note that regardless of the uptake mechanism, we found that C_{60}-serPF eventually localized to, and concentrated in, the nucleus.

Since entry into the nucleus is independent of the phase of the cell cycle, C_{60}-serPF must permeate through an intact nuclear envelope. Targeting approaches to deliver NPs to the nucleus of cells have taken advantage of the small size of NPs, or modifying them by conjugation with membrane-penetrating peptide sequences such as TAT or nuclear localization signals(44, 45). The dimensions of individual C_{60}-serPF particles are comparable to 2.1nm CdTe quantum dots that demonstrated passive, as well as active, entry into the nucleus(46). Although CdTe quantum dots were found to associate with positively charged histones upon nuclear entry, the docking of C_{60}-serPF onto proteins for nuclear entry is a unique phenomenon that will require further study. The data demonstrates that upon entry in the nucleus, C_{60}-serPF NPs accumulate, forming aggregates in association with chromatin. Unlike quantum dots, the location of these aggregates appears independent of the location of nucleoli (which stain lightly with DAPI). This fullerene aggregation may hinder elimination of C_{60}-serPF from the nucleus. Indeed, concentration-dependence of nuclear accumulation suggests that elimination of C_{60}-serPF aggregates from the nucleus fails to match the rate of nuclear entry at higher incubation concentrations.

It is possible that C_{60}-ser and its fluorophore conjugate, C_{60}-serPF, differ in their transport dynamics and hence their subcellular localization. Our efforts to detect C_{60}-ser using a commercially-available anti-C_{60} antibody (Santa Cruz Biotechnology) was unsuccessful because of the lack of affinity of this antibody for C_{60}-ser. Competitive inhibition using a 100-fold higher concentration of C_{60}-ser however, strongly suggests that C_{60}-serPF uptake in cancer cells follows pathways similar to that of C_{60}-ser.

CONCLUSIONS

We have demonstrated that a water-soluble, non-ionic derivatized-fullerene can localize to the nucleus and permeate into a wide variety of tissues, including malignant liver tumors and brain. These findings should have far reaching implications in designing nanovector-based drug delivery systems and diagnostic imaging agents that aim to exploit the unique combination of small nanoscale size, lipophilicity, and molecular topology of the fullerene cage. Future studies, already underway, will examine [60]fullerene derivatives of different structure and charge, with a special emphasis on nuclear envelope and brain-blood barrier transport.

Supplementary Material

Refer to Web version on PubMed Central for supplementary material.

Acknowledgments

This work was funded from the NIH (U54CA143837), NIH M. D Anderson Cancer Center Support Grant CA016672, and the V Foundation (SAC). We also gratefully acknowledge the Welch Foundation (grant C-0627) and the Kanzius Research Foundation for partial support of this work.

REFERENCES

1. Kroto HW, Heath JR, Obrien SC, Curl RF, Smalley RE. C-60 - buckminsterfullerene. Nature. 1985; 318(6042):162–3.
2. Sengupta S, Chaudhuri P, Paraskar A, Soni S, Mashelkar RA. Fullerenol cytotoxic conjugates for cancer chemotherapy. Acs Nano. Sep; 2009 3(9):2505–14. [PubMed: 19681636]
3. Wilson LJ, Zakharian TY, Seryshev A, Sitharaman B, Gilbert BE, Knight V. A fullerene-paclitaxel chemotherapeutic: synthesis, characterization, and study of biological activity in tissue culture. J Am Chem. 2005; 127(36):12508–9.
4. Nakamura E, Isobe H, Nakanishi W, Tomita N, Jinno S, Okayama H. Nonviral gene delivery by tetraamino fullerene. Mol Pharm. 2006; 3(2):124–34. [PubMed: 16579641]
5. Nakamura E, Isobe H, Nakanishi W, Tomita N, Jinno S, Okayama H. Gene delivery by aminofullerenes: structural requirements for efficient transfection. Chem-Asian J. 2006; 1(1-2):167–75. [PubMed: 17441052]
6. Hamblin MR, Mroz P, Pawlak A, Satti M, Lee H, Wharton T, et al. Functionalized fullerenes mediate photodynamic killing of cancer cells: type I versus type II photochemical mechanism. Free Radical Bio Med. 2007; 43(5):711–9. [PubMed: 17664135]
7. Hamblin MR, Mroz P, Tegos GP, Gali H, Wharton T, Sarna T. Photodynamic therapy with fullerenes. Photoch Photobio Sci. 2007; 6(11):1139–49.
8. Ikeda A, Doi Y, Akiyama M, Nagano M, Shigematsu T, Ogawa T, et al. Intracellular uptake and photodynamic activity of water-Soluble [60]- and [70]fullerenes incorporated in liposomes. Chem-Eur J. 2008; 14(29):8892–7. [PubMed: 18698574]
9. Ikeda A, Sue T, Akiyama M, Fujioka K, Shigematsu T, Doi Y, et al. Preparation of highly photosensitizing liposomes with fullerene-doped lipid bilayer using dispersion-controllable molecular exchange reactions. Org Lett. 2008; 10(18):4077–80. [PubMed: 18707108]
10. Krishna V, Stevens N, Koopman B, Moudgil B. Optical heating and rapid transformation of functionalized fullerenes. Nat Nanotechnol. 2010; 5(5):330–4. [PubMed: 20228785]
11. Lens M, Medenica L, Citernesi U. Antioxidative capacity of C(60) (buckminsterfullerene) and newly synthesized fulleropyrrolidine derivatives encapsulated in liposomes. Biotechnol Appl Bioc. 2008; 51:135–40.
12. Citrin DE, Brown AP, Chung EJ, Urick ME, Shield WP, Sowers AL, et al. Evaluation of the fullerene compound DF-1 as a radiation protector. Radiat Oncol. 2010; 5

13. Dicker AP, Daroczi B, Kari G, McAleer MF, Wolf JC, Rodeck U. In vivo radioprotection by the fullerene nanoparticle DF-1 as assessed in a zebrafish model. Clin Cancer Res. 2006; 12(23): 7086–91. [PubMed: 17145832]
14. Wilson LJ, Sitharaman B, Tran LA, Pham QP, Bolskar RD, Muthupillai R, et al. Gadofullerenes as nanoscale magnetic labels for cellular MRI. Contrast Media Mol I. 2007; 2(3):139–46.
15. Wilson LJ, Wharton T. Highly-iodinated fullerene as a contrast agent for x-ray imaging. Bioorgan Med Chem. 2002; 10(11):3545–54.
16. Larroque C, Foley S, Crowley C, Smaihi M, Bonfils C, Erlanger BF, et al. Cellular localisation of a water-soluble fullerene derivative. Biochem Bioph Res Co. 2002; 294(1):116–9.
17. Pincelli C, Chirico F, Fumelli C, Marconi A, Tinari A, Straface E, et al. Carboxyfullerenes localize within mitochondria and prevent the UVB-induced intrinsic apoptotic pathway. Exp Dermatol. 2007; 16(5):429–36. [PubMed: 17437486]
18. Chen CY, Li W, Ye C, Wei TT, Zhao YL, Lao F, et al. The translocation of fullerenic nanoparticles into lysosome via the pathway of clathrin-mediated endocytosis. Nanotechnology. 2008; 19(14)
19. Kepley CL, Dellinger A, Zhou ZG, Norton SK, Lenk R, Conrad D. Uptake and distribution of fullerenes in human mast cells. Nanomed-Nanotechnol. 2010; 6(4):575–82.
20. Wilson LJ, Wharton T, Kini VU, Mortis RA. New non-ionic, highly water-soluble derivatives of C-60 designed for biological compatibility. Tetrahedron Lett. 2001; 42(31):5159–62.
21. Bachas LG, Nednoor P, Capaccio M, Gavalas VG, Meier MS, Anthony JE. Hybrid nanoparticles based on organized protein immobilization on fullerenes. Bioconjugate Chem. 2004; 15(1):12–5.
22. Gozin M, Belgorodsky B, Fadeev L, Ittah V, Benyamini H, Zelner S, et al. Formation and characterization of stable human serum albumin-tris-malonic acid [C-60]fullerene complex. Bioconjugate Chem. 2005; 16(5):1058–62.
23. Wilson LJ, Ashcroft JM, Tsyboulski DA, Hartman KB, Zakharian TY, Marks JW, et al. Fullerene (C-60) immunoconjugates: interaction of water-soluble C-60 derivatives with the murine anti-gp240 melanoma antibody. Chem Commun. 2006; (28):3004–6.
24. Schmid SL, Conner SD. Regulated portals of entry into the cell. Nature. 2003; 422(6927):37–44. [PubMed: 12621426]
25. Ivanov, AI. Exocytosis and endocytosis. Humana Press; Totowa, N.J.: 2008.
26. Amyere M, Mettlen M, Van Der Smissen P, Platek A, Payrastre B, Veithen A, et al. Origin, originality, functions, subversions and molecular signalling of macropinocytosis. Int J Med Microbiol. 2002; 291(6-7):487–94. [PubMed: 11890548]
27. Nakase I, Niwa M, Takeuchi T, Sonomura K, Kawabata N, Koike Y, et al. Cellular uptake of arginine-rich peptides: roles for macropinocytosis and actin rearrangement. Mol Ther. 2004; 10(6): 1011–22. [PubMed: 15564133]
28. Veithen A, Cupers P, Baudhuin P, Courtoy PJ. v-src induces constitutive macropinocytosis in rat fibroblasts. J Cell Sci. 1996; 109(Pt 8):2005–12. [PubMed: 8856496]
29. Hinshaw JE, Schmid SL. Dynamin self-assembles into rings suggesting a mechanism for coated vesicle budding. Nature. 1995; 374(6518):190–2. [PubMed: 7877694]
30. Kelly RB. Endocytosis. Ringing necks with dynamin. Nature. 1995; 374(6518):116–7. [PubMed: 7877678]
31. Roux A, Uyhazi K, Frost A, De Camilli P. GTP-dependent twisting of dynamin implicates constriction and tension in membrane fission. Nature. 2006; 441(7092):528–31. [PubMed: 16648839]
32. Thompson HM, McNiven MA. Discovery of a new ‘dynasore’. Nat Chem Biol. 2006; 2(7):355–6. [PubMed: 16783339]
33. Yancey PG, Rodrigueza WV, Kilsdonk EP, Stoudt GW, Johnson WJ, Phillips MC, et al. Cellular cholesterol efflux mediated by cyclodextrins. Demonstration Of kinetic pools and mechanism of efflux. J Biol Chem. 1996; 271(27):16026–34. [PubMed: 8663188]
34. Ros-Baro A, Lopez-Iglesias C, Peiro S, Bellido D, Palacin M, Zorzano A, et al. Lipid rafts are required for GLUT4 internalization in adipose cells. P Natl Acad Sci USA. 2001; 98(21):12050–5.

35. Wang LH, Rothberg KG, Anderson RG. Mis-assembly of clathrin lattices on endosomes reveals a regulatory switch for coated pit formation. J Cell Biol. 1993; 123(5):1107–17. [PubMed: 8245121]
36. Cook A, Bono F, Jinek M, Conti E. Structural biology of nucleocytoplasmic transport. Annu Rev Biochem. 2007; 76:647–71. [PubMed: 17506639]
37. Perez-Terzic C, Pyle J, Jaconi M, Stehno-Bittel L, Clapham DE. Conformational states of the nuclear pore complex induced by depletion of nuclear Ca2+ stores. Science. 1996; 273(5283): 1875–7. [PubMed: 8791595]
38. Blair OC, Winward RT, Roti Roti JL. The effect of hyperthermia on the protein content of HeLa cell nuclei: a flow cytometric analysis. Radiat Res. 1979; 78(3):474–84. [PubMed: 377370]
39. Zeng XC, Bhasin S, Wu X, Lee JG, Maffi S, Nichols CJ, et al. Hsp70 dynamics in vivo: effect of heat shock and protein aggregation. J Cell Sci. 2004; 117(Pt 21):4991–5000. [PubMed: 15367583]
40. Salonen E, Lin S, Reid ML, Allegood M, Wang X, Rao AM, et al. Real-Time translocation of fullerene reveals cell contraction. Small. 2008; 4(11):1986–92. [PubMed: 18949789]
41. Porter AE, Muller K, Skepper J, Midgley P, Welland M. Uptake of C-60 by human monocyte macrophages, its localization and implications for toxicity: Studied by high resolution electron microscopy and electron tomography. Acta Biomater. 2006; 2(4):409–19. [PubMed: 16765881]
42. Cokakli M, Erdal E, Nart D, Yilmaz F, Sagol O, Kilic M, et al. Differential expression of Caveolin-1 in hepatocellular carcinoma: correlation with differentiation state, motility and invasion. BMC Cancer. 2009; 9:65. [PubMed: 19239691]
43. Prescott JL, Tindall DJ. Clathrin gene expression is androgen regulated in the prostate. Endocrinology. 1998; 139(4):2111–9. [PubMed: 9529000]
44. Fuente JM, Berry CC. Tat peptide as an efficient molecule to translocate gold nanoparticles into the cell nucleus. Bioconjugate Chem. 2005; 16(5):1176–80.
45. Sun SH, Xu CJ, Xie J, Kohler N, Walsh EG, Chin YE. Monodisperse magnetite nanoparticles coupled with nuclear localization signal peptide for cell-nucleus targeting. Chem-Asian J. 2008; 3(3):548–52. [PubMed: 18080259]
46. Nabiev I, Mitchell S, Davies A, Williams Y, Kelleher D, Moore R, et al. Nonfunctionalized nanocrystals can exploit a cell's active transport machinery delivering them to specific nuclear and cytoplasmic compartments. Nano Lett. 2007; 7(11):3452–61. [PubMed: 17949046]

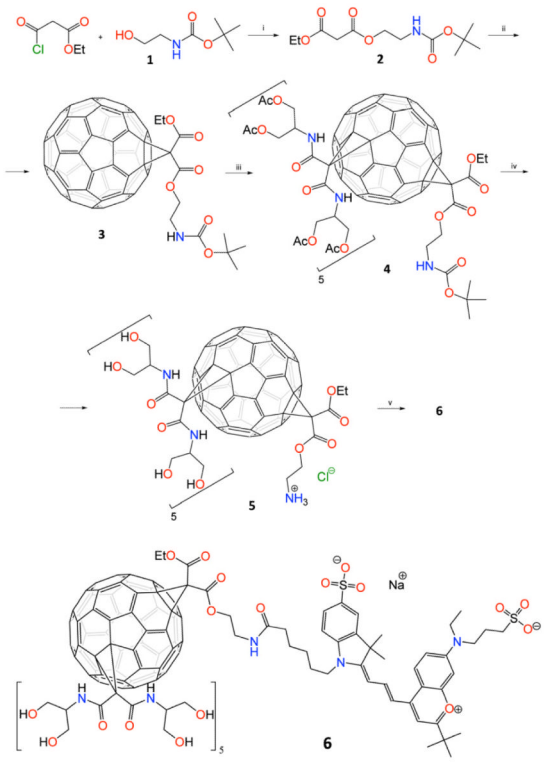

Figure 1. Synthesis of fullerene[60] serinol malonate pentakis-adduct – PromoFluor-633 conjugate (6)

(i) Hünig's base, in dry CH_2Cl_2, −20 °C → RT, 6 h. (ii) C_{60}, CBr_4, DBU, 4 h. (iii) 3, CBr_4, base P_1-*t*-Bu, 24 h. (iv) 1M HCl in dioxane: water = 99:1, RT, 48 h. (v) PF-633 carboxylic acid, EDC, HOBt Hydrate, MES buffer, 30 min.

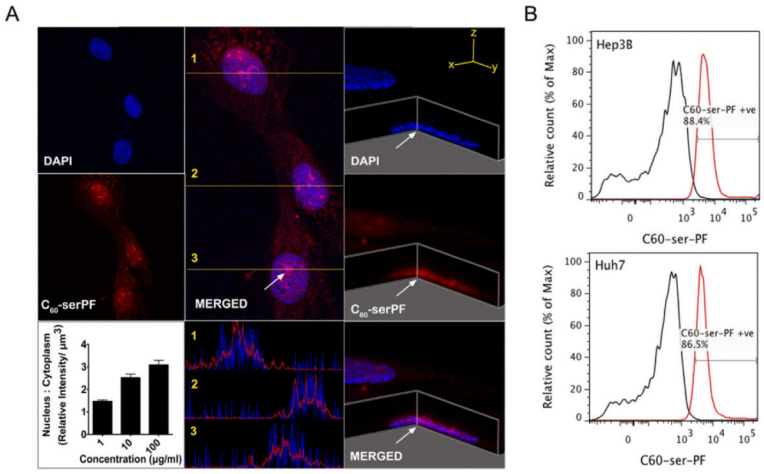

Figure 2. C_{60}-serPF NPs localize to the nucleus liver cancer cells

Panel A. Confocal microscopy image of Hep3B cells and Z-stack through the nucleus at the point depicted by the arrow. Intensity profiles through line 1, 2, and 3 are also represented, demonstrating colocalization with DAPI. Concentration of C_{60}-serPF in the nucleus increases relative to cytoplasm as the cells are exposed to increasing concentrations of C_{60}-serPF. Panel B. Nuclear uptake is confirmed by flow cytometry after extraction of nuclei demonstrating uptake in the majority of cells.

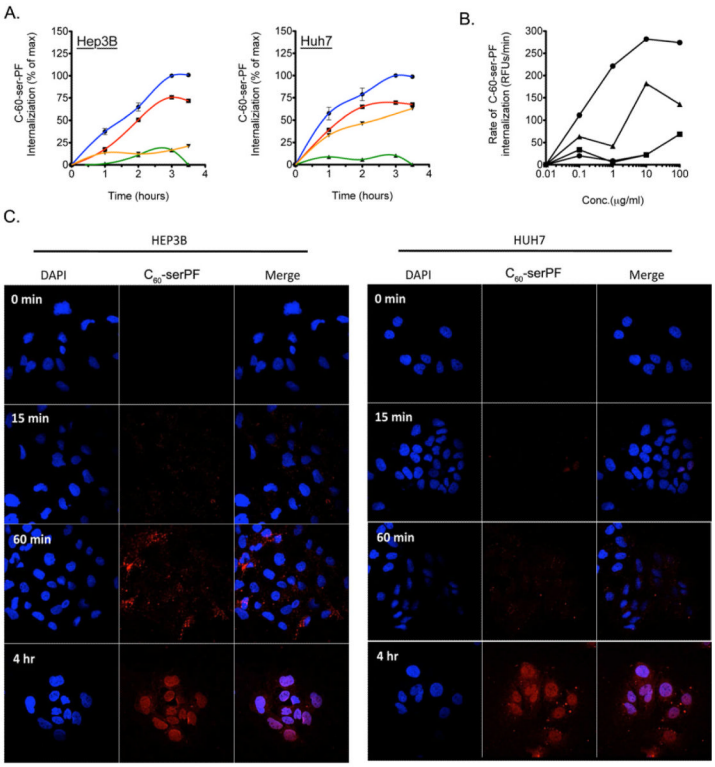

Figure 3. Internalization dynamics of C_{60}-serPF in liver cancer cell lines

Panel A. Cellular uptake of C_{60}-serPF in Hep3B and Huh7 cells is inhibited at 4°C (green) or by 1-hr pre-incubation with C_{60}-ser, 10x (red) or 100x (orange), at 37°C in comparison with controls (blue). Panel B. Rate of internalization in Hep3B cells demonstrates saturation kinetics at 10μg/ml in control cells at 37°C (●) and is inhibited by incubation at 4°C (■) or by removal of serum proteins at 37°C (▲), or at 4°C (▼). Panel C. Time course of entry of C_{60}-serPF into the nucleus of Hep3B (left) and Huh7 (right) cells

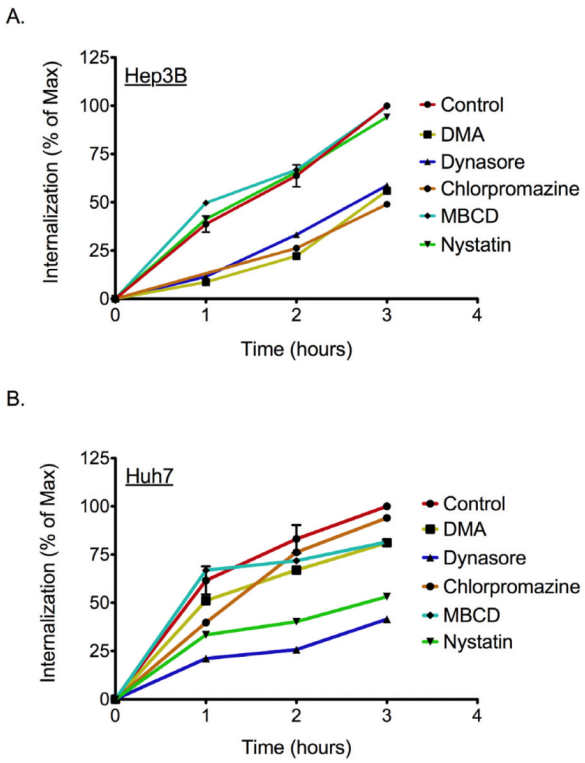

Figure 4. Pathways of cellular uptake for C_{60}-serPF

Panel A. C_{60}-serPF internalization in Hep3B cells is susceptible to inhibitors of macropinocytosis (DMA) and dynamin-dependent, clathrin-mediated pathway (dynamin and chlorpromazine). Panel B. Uptake of C_{60}-serPF in Huh7 cells is inhibited by inhibitors of macropinocytosis (DMA) and dynamin-dependent, caveolin/ lipid-raft-mediated pathway (Dynamin, nystatin and MBCD).

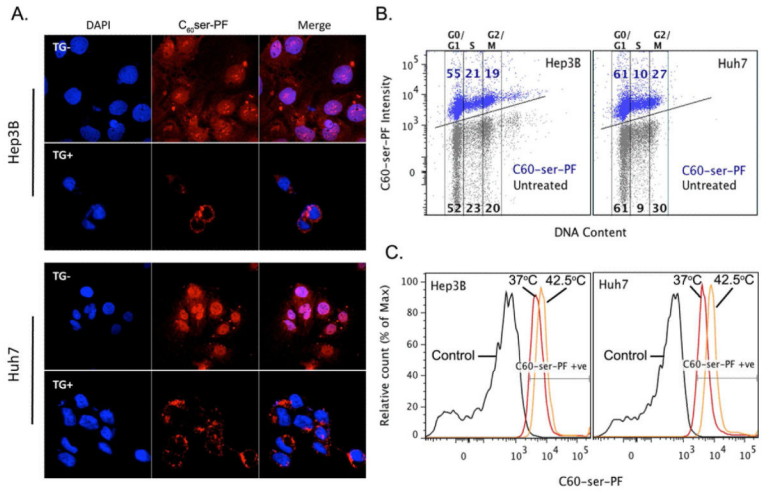

Figure 5. Mechanism of nuclear uptake

Nuclear uptake of C_{60}-serPF in Hep3B and Huh7 cells is inhibited by thapsigargin (TG), panel A and is independent of cell cycle kinetics, panel B. Nuclear uptake of C_{60}-serPF is enhanced under hyperthermic conditions (42.5°C), panel C, suggesting active and passive transport across the nuclear pore complex.

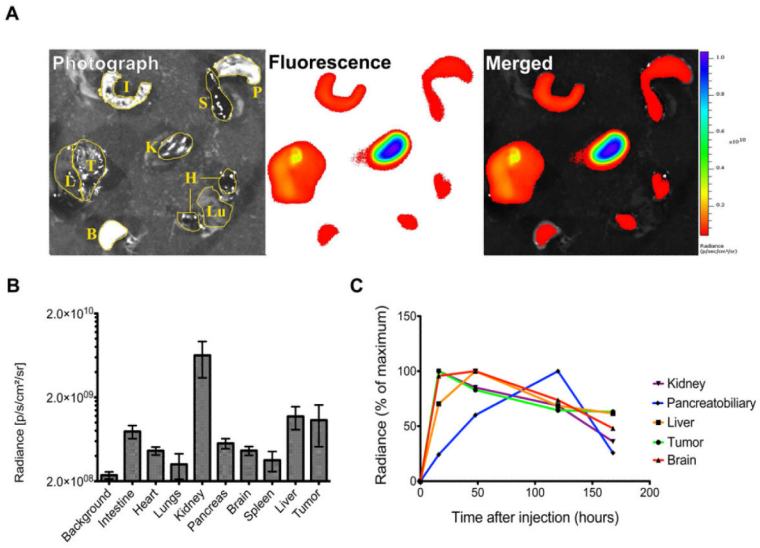

Figure 6. Relative biodistribution of C_{60}-serPF in an animal model of primary liver cancer and *in vivo* nuclear localization

Panel A. Fluorescence images from tumor (T), Liver (L), Intestine (I), Pancreatobiliary (P), Spleen (S), Kidney (K), Brain (B), bisected heart (H), and Lungs (Lu) of a mouse bearing an orthotopic liver tumor generated after injecting Hep3B cells into the liver. Panel B. Relative tissue distribution of C_{60}-serPF in mouse tissues, demonstrating accumulation in most tissues at 16-hours and predominantly in the kidney, liver, and liver cancer. (n=3) Panel C. Pharmacokinetics of fullerene uptake in select tissues, suggesting early renal clearance and a delayed hepatic clearance. C_{60}-serPF localizes to the brain and tumor within 16 hours and persists for more than one week (one mouse per time point represented).